Cell

Retinoic Acid from the Meninges Regulates Cortical Neuron Generation

Julie A. Siegenthaler,[1] Amir M. Ashique,[3,7] Konstantinos Zarbalis,[1,7] Katelin P. Patterson,[1] Jonathan H. Hecht,[1,2] Maureen A. Kane,[4] Alexandra E. Folias,[4] Youngshik Choe,[1] Scott R. May,[6] Tsutomu Kume,[5,8] Joseph L. Napoli,[4] Andrew S. Peterson,[3] and Samuel J. Pleasure[1,*]

[1]Department of Neurology, Programs in Neuroscience and Developmental Biology, Institute for Regenerative Medicine
[2]Department of Pediatrics
University of California San Francisco, San Francisco, CA 94158, USA
[3]Genentech, Inc. Department of Molecular Biology, South San Francisco, CA 94080, USA
[4]Department of Nutritional Science and Toxicology, University of California Berkeley, Berkeley, CA 94720, USA
[5]Division of Cardiovascular Medicine, Vanderbilt University Medical Center, Nashville, TN 37232, USA
[6]The Salk Institute for Biological Studies, San Diego, CA 92186, USA
[7]These authors contributed equally to this work
[8]Present address: Feinberg Cardiovascular Research Institute, Northwestern University School of Medicine, Chicago, IL 60611, USA
*Correspondence: sam.pleasure@ucsf.edu
DOI 10.1016/j.cell.2009.10.004

SUMMARY

Extrinsic signals controlling generation of neocortical neurons during embryonic life have been difficult to identify. In this study we demonstrate that the dorsal forebrain meninges communicate with the adjacent radial glial endfeet and influence cortical development. We took advantage of *Foxc1* mutant mice with defects in forebrain meningeal formation. *Foxc1* dosage and loss of meninges correlated with a dramatic reduction in both neuron and intermediate progenitor production and elongation of the neuroepithelium. Several types of experiments demonstrate that retinoic acid (RA) is the key component of this secreted activity. In addition, *Rdh10*- and *Raldh2*-expressing cells in the dorsal meninges were either reduced or absent in the *Foxc1* mutants, and *Rdh10* mutants had a cortical phenotype similar to the *Foxc1* null mutants. Lastly, in utero RA treatment rescued the cortical phenotype in *Foxc1* mutants. These results establish RA as a potent, meningeal-derived cue required for successful corticogenesis.

INTRODUCTION

Early in cerebral cortical development, lateral expansion of the cortical neuroepithelium dominates as neuroepithelial progenitors in the ventricular zone (VZ), the radial glial cells, symmetrically divide with both daughter cells re-entering the cell cycle. As corticogenesis proceeds, the radial expansion of the cortex begins as VZ progenitors divide asymmetrically to generate postmitotic neurons directly or intermediate progenitor cells (IPCs) destined for additional, neuron-generating divisions in the subventricular zone (SVZ) (Chenn and McConnell, 1995; Miyata et al., 2004; Noctor et al., 2004, 2008). The balance of lateral and radial expansion of the neocortex depends upon the appropriately timed switch from symmetric to asymmetric divisions. Intrinsic (transcription factors, asymmetric protein distribution, etc.) and extrinsic factors (growth factors and other diffusible ligands) are implicated in the mechanics of this switch, most of which localize to cells in cortical neuroepithelium (Chenn and McConnell, 1995; Chenn and Walsh, 2002; Kawaguchi et al., 2004; Li et al., 1998; Qian et al., 1997). The factors that control the timing and continued progression of cortical neurogenesis, however, have remained largely obscure. Here we present evidence that all-trans retinoic acid (atRA) released from the meninges is involved in the decision of neuroepithelial cells to generate IPCs and neurons.

atRA is a hormone derived from vitamin A (retinol) that signals via binding to its nuclear retinoic acid receptors (RAR) and retinoid X receptors (RXR) (Chambon, 1996). atRA synthesis is a two-step process that requires retinol dehydrogenases (Rdh) and retinaldehyde dehydrogenases (Raldh1, 2, and 3) (Napoli, 2004; Ross et al., 2000). Raldh2 is critical for atRA synthesis in the developing embryo; *Raldh2*$^{-/-}$ embryos are almost entirely devoid of atRA signaling and die around E9.5–E10.5 with defects in head, trunk, and heart development (Niederreither et al., 1999). Adequate atRA production during development also depends upon the activity of Rdh10 as demonstrated by the dramatic reduction in atRA levels in the *Rdh10* hypomorph, which displays head, limb, and organ defects typical of severe atRA deficiency (Sandell et al., 2007).

Early forebrain morphogenesis requires atRA signaling (Ribes et al., 2006), and at these early patterning stages the source of atRA is the adjacent forming eye and nasal pits that express Raldh2 and Raldh3 (Anchan et al., 1997; Molotkova et al., 2007). Even as these rich sources of atRA become spatially disparate from the dorsal forebrain, there is evidence of strong and very specific atRA signaling in the cortical radial glial progenitors. This has been perplexing largely because even though RARα and RXRα, β are expressed in the cortical neuroepithelium (Dolle et al., 1994; Ruberte et al., 1993), the enzymes required for

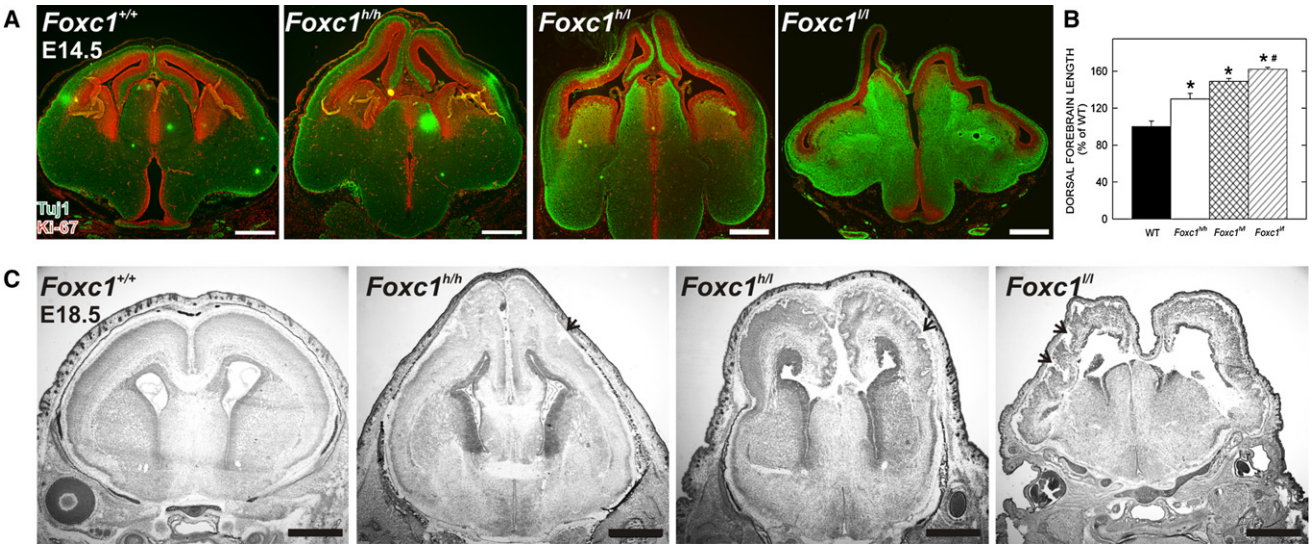

Figure 1. *Foxc1* Gene Dosage Correlates with Severity of Dorsal Forebrain Phenotype

(A) E14.5 *Foxc1*$^{+/+}$, *Foxc1*$^{h/h}$, *Foxc1*$^{h/l}$, and *Foxc1*$^{l/l}$ forebrains labeled with Tuj1 (green) and Ki-67 (red).

(B) Quantification of the dorsal forebrain length in WT and *Foxc1*$^{h/h}$, *Foxc1*$^{h/l}$, and *Foxc1*$^{l/l}$ brains.

(C) Nissl stains of E18.5 *Foxc1*$^{h/h}$, *Foxc1* $^{h/l}$, and *Foxc1*$^{l/l}$ mutant brains. Arrows indicate cortical dysplasia.

Scale bars = 500 μm (A) and 1 mm (C). * and # denote statistical significance ($p < 0.05$) from WT and *Foxc1*$^{h/h}$, respectively. Error bars depict ± the standard error of the mean (SEM).

atRA synthesis are not expressed in the dorsal forebrain and, consequently, the functional role of atRA during corticogenesis has been largely neglected. In this study we show that mice that fail to form complete forebrain meninges, *Foxc1* mutants (Vivatbutsiri et al., 2008; Zarbalis et al., 2007), have major defects in the switch from lateral VZ expansion to neuronogenic radial expansion of the cortex, and this is due to a loss of meningeal-derived atRA.

RESULTS

Reduction or Loss of *Foxc1* Leads to Lateral Expansion of the Dorsal Forebrain and Decreased Neuron Production

We previously identified a hypomorphic allele of the *Foxc1* gene (*Foxc1*^{hith}) with perinatal cortical dysplasia due to defects in the basement membrane and meningeal differentiation (Zarbalis et al., 2007). These *Foxc1* hypomorphs displayed an earlier cortical phenotype characterized by a longer dorsal forebrain. To fully characterize this phenotype we analyzed an allelic series of *Foxc1* mutants: *Foxc1* hypomorphs (*Foxc1*$^{hith/hith}$; *Foxc1*$^{h/h}$), a hypomorph-null hybrid (*Foxc1*$^{hith/lacZ}$; *Foxc1*$^{h/l}$), and *Foxc1* null embryos (*Foxc1*$^{lacZ/lacZ}$; *Foxc1*$^{l/l}$) (Kume et al., 1998). At E14.5, the dorsal forebrain was significantly longer ($p < 0.05$; Figure 1B) and appeared thinner in all three *Foxc1* mutants compared to the wild-type (WT) with the phenotype worsening with decreased gene dosage (Figure 1A). At E10.5 there was no cortical phenotype in any of the *Foxc1* mutant lines (Figure S1A available online); however, by E12.5 dorsal forebrain lengthening was evident (Figure S1B). The extended cortical wall translated into cortical dysplasia that ranged from moderate to severe at E18.5 (Figure 1C).

The lateral expansion of the neuroepithelium in the *Foxc1* mutants suggests a predominance of symmetric divisions. We looked at this indirectly by analyzing expression of atypical-PKCλ (aPKCλ) and Par3, proteins that are enriched at the apical membrane of neuroepithelial cells undergoing symmetric divisions (Costa et al., 2008). In WT brains at E14.5, aPKCλ was present at low levels in the apical membrane of VZ progenitors along the ventricular surface with a few areas of bright apical staining (Figure 2A). In all three *Foxc1* mutant cortices, aPKCλ levels were significantly ($p < 0.05$) elevated (Figures 2A and 2C). Although less abundant, apical Par3 was also significantly ($p < 0.05$) increased in all *Foxc1* mutants with the *Foxc1*$^{l/l}$ mutants having the largest increase (Figures 2B and 2C).

We next measured the output of asymmetric divisions, neurons and IPCs. A bromodeoxyuridine (BrdU)/Ki-67 cell-cycle exit assay was used to examine neuron generation. BrdU-positive (BrdU^{+}) but Ki-67-negative (Ki-67^{-}) cells were counted as cells that had exited the cell cycle. In WT cortex, a band of BrdU^{+}/Ki-67^{-} cells was apparent above the SVZ (Figure 2D; above dotted line). All three mutants had significantly ($p < 0.05$) reduced BrdU^{+}/Ki-67^{-} populations though the *Foxc1*$^{h/h}$ was less affected than the *Foxc1*$^{h/l}$ and *Foxc1*$^{l/l}$ mutants (Figures 2E–2H). Tbr2 immunolabeling was used to examine the IPC population. Significant ($p < 0.05$) reductions in Tbr2^{+} cell number were observed in all three *Foxc1* mutants (Figures 2I–2M) with the *Foxc1* null having the most severe deficit (Figure 2L). At E14.5, the decrease in cell-cycle exit (and presumably, to a lesser extent, the decrease in IPCs) correlated with a decrease in Ctip2^{+}, postmitotic neurons in the *Foxc1* mutants (Figures 2N–2Q).

To determine the consequences of the decreased production of neurons and IPCs in older embryos, we examined expression

of a deep (Ctip2) and a superficial cortical layer marker (Brn2) at E18.5. In all the *Foxc1* mutants (Figures 2S–2U), the cortical layers were disorganized (Figure 2R). Like at E14.5, the Ctip2$^+$ cell population was progressively and dramatically reduced in number according to genotype. The Brn2 population in the VZ, SVZ, and upper cortical layers was even more affected with very few Brn2$^+$ cells present in the superficial cortex of the *Foxc1*$^{l/l}$ brain (Figure 2U).

The decrease in neuron output and IPC production in the *Foxc1* mutants could be caused by defects in forebrain patterning or the VZ progenitor population, a change in cell cycle, or radial glia detachment. Expression of dorsal forebrain-restricted Pax6 and Tbr2 highlighted the elongation of the dorsal forebrain, but both were present in a normal spatial distribution (Figure S1C). Closer examination of Pax6, expressed by neuronal progenitors in the VZ, showed that the thickness of the Pax6$^+$ layer appeared normal in all the *Foxc1* mutants (Figure S1D). The Pax6 expression coupled with the increased length of the mutant cortices (and thus the neuroepithelium) provides additional evidence that the neuronal progenitor population is increased in the *Foxc1* mutants. Cell-cycle analysis in the VZ (S phase and total length of the cell cycle) at E14.5 showed no overt differences in either parameter between WT and any of the *Foxc1* mutants (Figure S1E). We also found no evidence of increased apoptotic cell death at E14.5 or E18.5 (data not shown). Finally, because of previous work describing basement membrane disruptions and radial glial detachment in the *Foxc1*$^{h/h}$ brains at E18.5 (Zarbalis et al., 2007), we examined laminin and nestin expression in the *Foxc1*$^{l/l}$ at E13.5. At this age, the dorsal forebrain phenotype was apparent, but there was no evidence of disruption in the basement membrane in the *Foxc1*$^{l/l}$ cortex and the radial glial processes appeared well organized (Figures S1F and S1G). In both WT and *Foxc1*$^{1/l}$ cortices, the radial glial endfeet colocalized with laminin at the *glia limitans* (Figure S1G, insets) and high-power, confocal images did not reveal radial glial detachment in the *Foxc1*$^{l/l}$ cortex (Figure S1H).

The Dorsal Forebrain Meninges Are Reduced or Absent in *Foxc1* Mutants

The meninges are directly opposed to the radial glial endfeet of the VZ progenitors, thus making them a potential root cause of the cortical phenotype in the *Foxc1* mutants. To examine the distribution of meningeal fibroblasts in the *Foxc1* mutants, we used an antibody that recognizes Zic protein family members that are expressed by meningeal fibroblasts (Inoue et al., 2008). In the E14.5 WT brain, Zic$^+$ meningeal cells completely surrounded the forebrain (Figure 3A). Zic$^+$ meningeal cells as well as Zic$^+$ Cajal-Retzius cells in the marginal zone of the brain were evident at higher magnification (Figure 3A′). The Zic$^+$ meningeal cells were present in ventral and lateral meninges of the *Foxc1*$^{h/h}$ brain, but bright, Zic$^+$ meningeal cells were absent in the most dorsal meninges (Figures 3B and 3B′). In the *Foxc1*$^{h/l}$ brain, Zic$^+$ meningeal cells covered only a short portion of the lateral cerebral wall (Figures 3C and 3C′). The Zic$^+$ meninges in the *Foxc1*$^{l/l}$ were completely missing over the dorsal forebrain but were present ventrally (Figures 3D and 3D′). To confirm that the Zic labeling reflected a loss of meninges and not just the loss of Zic expression, we looked at β-galactosidase (β-gal) activity in *Foxc1*$^{l/+}$ and *Foxc1*$^{l/l}$. In the *Foxc1*$^{l/+}$, darkly labeled β-gal$^+$ meningeal cells were present in a continuous layer around the brain and more lightly labeled vascular cells were evident in brain tissue (Figures 3E and 3E′). In contrast, the darkly labeled β-gal$^+$ meningeal cells in *Foxc1*$^{l/l}$ brains ended below the ventral forebrain leaving only β-gal$^+$ vascular cells in the supracortical mesenchyme (Figures 3F and 3F′).

The Meninges Secrete a Diffusible Factor that Promotes Cell-Cycle Exit

The progressive decrease in neuron and IPC production as meningeal coverage declines suggests that the cortical phenotype in the *Foxc1* mutants reflects a graded loss in a meningeal signal that influences the behavior of radial glial progenitors. To test this idea we performed two types of rescue experiments using E13.5 forebrain explants (Figure 4A): (1) transplantation of *Foxc1*$^{h/h}$ forebrain into normal meninges and (2) coculturing of *Foxc1*$^{h/h}$ explants with Foxc1$^+$/Zic$^+$ meningeal cells (Figures S2A and S2B) that conditioned the shared media.

Consistent with the in vivo experiments, untreated (i.e., no transplantation and no conditioned media) *Foxc1*$^{h/h}$ forebrain explants had a significantly ($p < 0.05$) reduced proportion of BrdU$^+$/Ki-67$^-$ cells (Figures 4B, 4C, and 4N). Meningeal transplantation did not affect cell-cycle exit in the *Foxc1*$^{+/}$ slices (Figures 4D and 4H); however cell-cycle exit was improved in the *Foxc1*$^{h/h}$ forebrain explants transplanted into the meningeal "ghosts" derived from *Foxc1*$^{+/}$ forebrain (Figures 4E and 4N). Similarly, coculturing *Foxc1*$^{h/h}$ forebrain explants with meningeal cells also significantly ($p < 0.05$) increased the proportion of BrdU$^+$/Ki-67$^-$ cells but did not affect cell-cycle exit in the *Foxc1*$^{+/}$ forebrain explants (Figures 4F, 4G, and 4N).

atRA Is the Bioactive Component of Meningeal Conditioned Medium and atRA Biosynthetic Enzymes Are Missing from the Meninges in the *Foxc1* Mutant Mice

atRA is a potent neuronal differentiation signal and enzymes required for atRA synthesis are expressed in the meninges, making it an attractive candidate molecule as the meningeal factor. Treatment with atRA (10 μM) did not affect cell-cycle exit in the *Foxc1*$^{+/}$ explants but increased cell-cycle exit in the cortex of *Foxc1*$^{h/h}$ explants (Figures 4H, 4I, and 4N). We next determined whether atRA is a required component of meningeal conditioned media for rescue of *Foxc1*$^{h/h}$ slices. We cocultured meningeal cells and slices in media with B27 supplement that lacked vitamin A (B27-VA), the precursor used to make atRA. In addition, we cultured slices in meningeal conditioned media that had been exposed to sunlight to deplete the atRA. To confirm that atRA was decreased, atRA levels were assayed by liquid chromatography tandem mass spectrometry (LC/MS/MS) (Kane et al., 2005, 2008) (Figure S2C). B27-VA conditioned media and atRA-depleted conditioned media did not alter cell-cycle exit in *Foxc1*$^{+/}$ slices (Figures 4J, 4L, and 4N), but both failed to rescue the cell-cycle exit phenotype in the *Foxc1*$^{h/h}$ slices (Figures 4K, 4M, and 4N). We did, however, notice an increased number of pyknotic nuclei in some *Foxc1*$^{+/}$ and *Foxc1*$^{h/h}$ explants cultured in meningeal conditioned media exposed to light (data not shown), which indicated increased cell

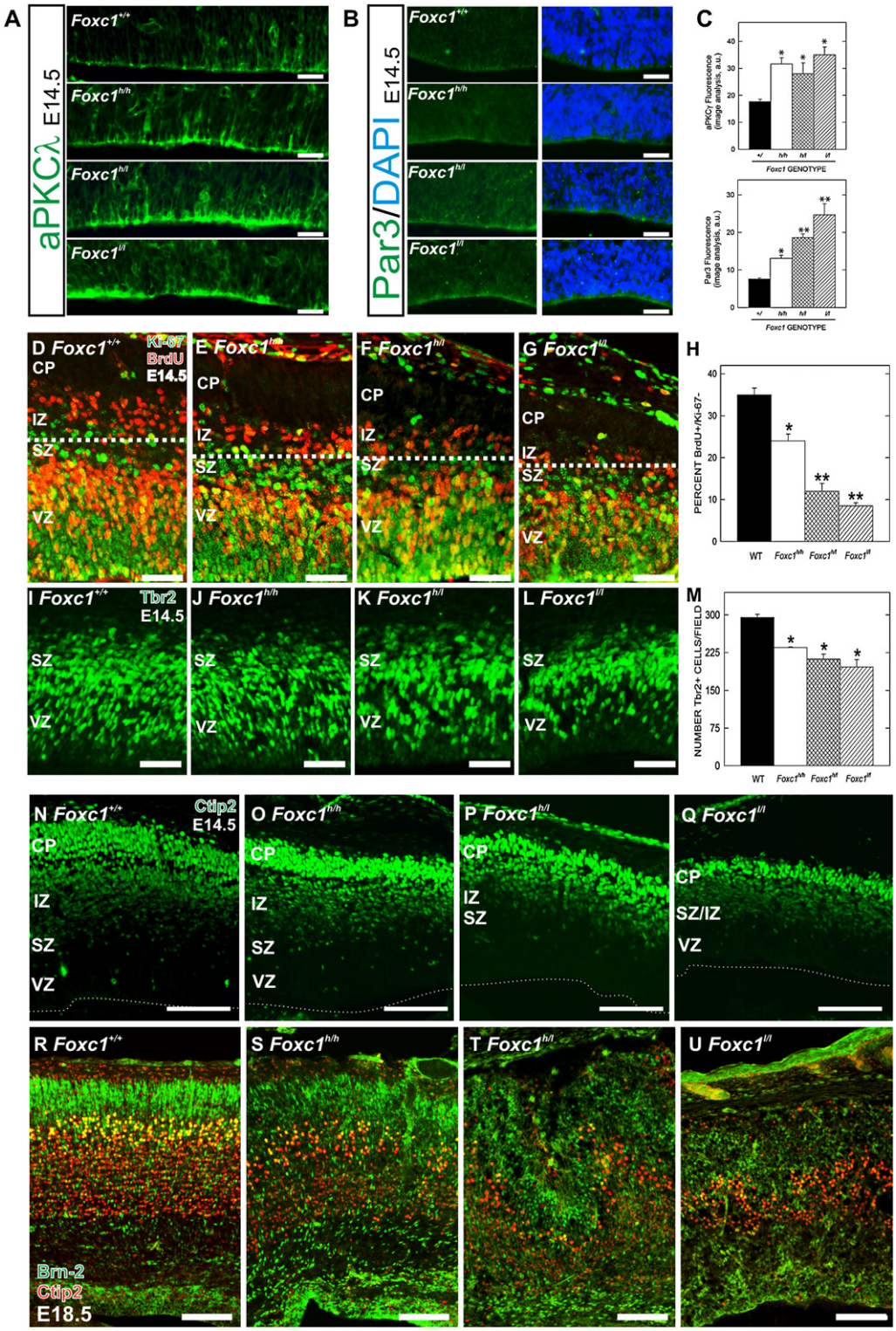

Figure 2. Defect in Switch from Symmetric to Asymmetric Divisions in the Neuroepithelium of *Foxc1* Mutants

(A) aPKCλ immunostaining in WT, *Foxc1*$^{h/h}$, *Foxc1*$^{h/l}$, and *Foxc1*$^{l/l}$ cortical neuroepithelium at E14.5.

(B) Par3 immunostaining (green) in the apical membrane of E14.5 WT, *Foxc1*$^{h/h}$, *Foxc1*$^{h/l}$, and *Foxc1*$^{l/l}$ cortical neuroepithelial cells with (right panels) and without (left panels) DAPI nuclear stain (blue).

(C) Quantification of fluorescent intensities of aPKCλ (top) and Par3 (bottom) in WT and *Foxc1* mutants.

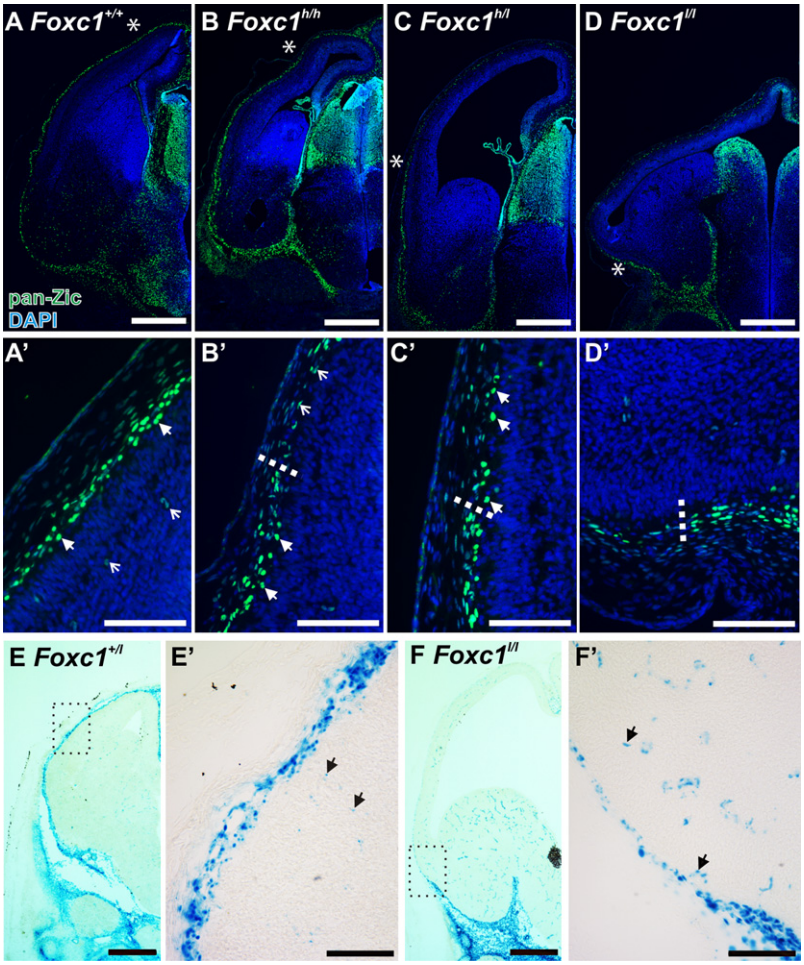

Figure 3. The Dorsal Forebrain Meninges Fail to Form Completely in the *Foxc1* Mutants

Low-magnification (A–D) and high-magnification (A′–D′) images of Zic immunostaining in WT, *Foxc1*$^{h/h}$, *Foxc1*$^{h/l}$, and *Foxc1*$^{l/l}$ E14.5 heads. Arrowheads in (A′), (B′), and (C′) indicate Zic^{+} Cajal-Retzius cells and open arrows in (A′) indicate Zic^{+} cells in the cortical vasculature. The endpoint of the meninges (denoted by an asterisk in B, C, and D) is shown in higher magnification view in (B′), (C′), and (D′) and indicated by a dotted line. Lightly labeled Zic^{+} vascular cells persist in the residual mesenchyme in all mutants (open arrows in B′).

Low-magnification (E and F) and high-magnification (E′ and F′) images of x-gal staining in E14.5 *Foxc1*$^{+/l}$ and *Foxc1*$^{l/l}$. Higher-magnification images show lightly labeled β-gal^{+} cells in the cortical vasculature (E′ and F′; arrows). Scale bars = 500 μm (A–D , E, and F) and 100 μm (A′–D′, E′, and F′).

death. Cell-cycle exit in *Foxc1*$^{+/}$ explants in this treatment condition did not differ from unconditioned media, indicating that the change in cell viability was not influencing this parameter.

We next looked at the expression of Raldh2 and Rdh10, two enzymes critical for atRA synthesis, in WT and *Foxc1* mutant meninges. In situ hybridization in E14.5 WT tissue showed that *Raldh2* and *Rdh10* signal was very high in the meninges, with no expression of *Raldh2* evident in the dorsal forebrain and a very low level of expression of *Rdh10* in the cerebral wall (Figures 5A, 5A′, 5E, and 5E′). Unlike *Raldh2*, *Rdh10* signal was also present in the choroid plexus and in the cortical hem in WT, *Foxc1*$^{h/h}$, and *Foxc1*$^{h/l}$ brains; this is consistent with previous analysis of *Rdh10* expression in the embryonic brain (Romand et al., 2008). In the *Foxc1*$^{h/h}$ brain, *Raldh2* and *Rdh10* expression was detectable in ventral and lateral meninges, but the expression intensity was patchy in the dorsal meningeal areas (Figures 5B, 5B′, 5F, and 5F′). In addition, the intensity of the *Raldh2* and *Rdh10* signal was reduced in the *Foxc1*$^{h/h}$ meninges, though the intensity levels were similar to WT in the facial mesenchyme. Even fewer *Rdh10*- and *Raldh2*-expressing cells surrounded the brains of the *Foxc1*$^{h/l}$ (Figures 5C, 5C′, 5G, and 5G′) and *Foxc1*$^{l/l}$ (Figures 5D, 5D′, 5H, and 5H′) mutants, though there was expression in the residual, midline meninges.

Temporal and Spatial Appearance of Raldh2^{+} Cells in the Meninges Correlates with Neurogenic Gradient

To test whether the onset of the *Foxc1* mutant cortical phenotype (E12.5 in the *Foxc1*$^{h/h}$; E11.5 in the *Foxc1*$^{h/l}$ and *Foxc1*$^{l/l}$ mutants; data not shown) is temporally and spatially related to the normal appearance of Raldh2^{+} cells in the meninges, we examined Raldh2 protein expression in WT brains on E11.5, E12.5, and E14.5. At E11.5, no Raldh2 staining was present in the meninges but was evident around the developing nasal cavities (Figure 6A). By E12.5, Raldh2^{+} cells were present in the ventral meninges and a few Raldh2^{+} cells were present in the lateral but not dorsal meninges (Figures 6B and 6B′). This suggests that Raldh2^{+} cells appear in a lateral to medial gradient, which is the same distribution as the gradient for neuron production during this same period. By E14.5 the entire meninges contained Raldh2^{+} cells (Figure 6C). Colabeling of Raldh2 with Foxc1 or Foxc2 in the dorsal meninges showed that the Raldh2^{+} cells represent a subset of cells within the Foxc1^{+} meninges (Figure 6D). Foxc2, a close homolog of Foxc1 that localizes to cells in the dura

(D–H) Representative staining from BrdU (red)/Ki-67 (green) cell-cycle exit assay; dotted line demarcates BrdU^{+}/Ki-67^{-} cells in the intermediate zone (IZ) of WT (D) *Foxc1*$^{h/h}$ (E), *Foxc1*$^{h/l}$ (F), and *Foxc1*$^{l/l}$ (G) cortices. The percentage of exited cells was quantified for WT and *Foxc1* mutants (H).

(I–M) Tbr2 immunostaining of IPCs in the VZ and SVZ of WT (I), *Foxc1* $^{h/h}$ (J), *Foxc1* $^{h/l}$ (K), and *Foxc1*$^{l/l}$ (L) cortices. Quantification of Tbr2^{+} cells in all genotypes (M).

(N–Q) Ctip2 (green) in E14.5 (N) WT, (O) *Foxc1* $^{h/h}$, (P) *Foxc1*$^{h/l}$, and (Q) *Foxc1*$^{l/l}$ mutants. Dotted line denotes ventricular surface.

(R–U) Brn2 (green) and Ctip2 (red) colabeling in E18.5 (R) WT, (S) *Foxc1* $^{h/h}$, (T) *Foxc1* $^{h/l}$, and (U) *Foxc1*$^{l/l}$ mutants.

Scale bars = 25 μm (A and B), 100 μm (D–G, I–L), and 200 μm (N–U). * and ** denote a statistically significant difference ($p < 0.05$) from WT and both WT and *Foxc1*$^{h/h}$, respectively. Abbreviations: CP, cortical plate; IZ, intermediate zone; SVZ, subventricular zone; VZ, ventricular zone. Error bars depict ± SEM.

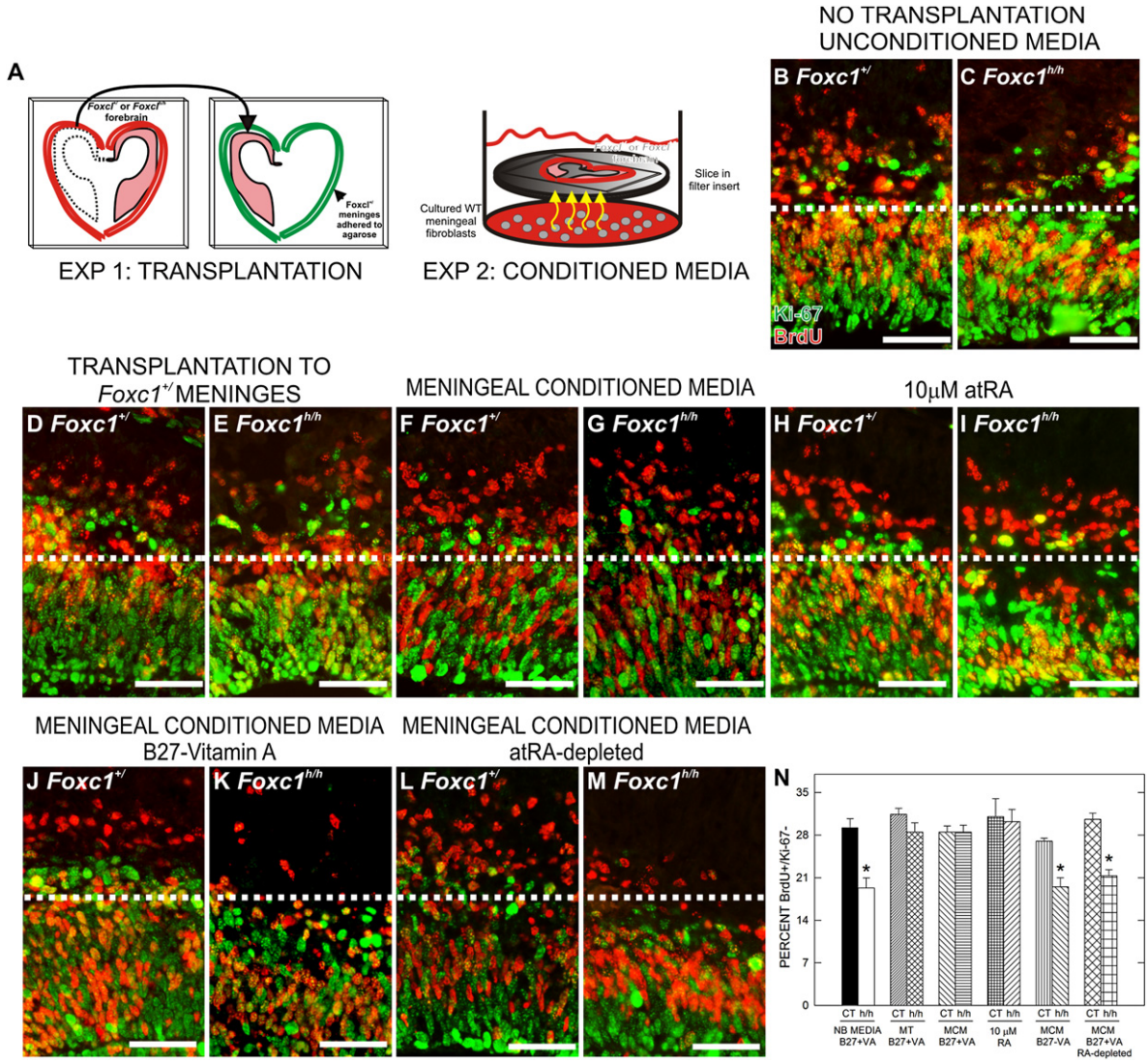

Figure 4. Cell-Cycle Exit Defect in *Foxc1*$^{h/h}$ Explants Is Rescued by Exposure to Secreted Cues from Meninges and atRA

(A) Depiction of in vitro explant preparations: meningeal transplantation preparation (left diagram) and coculturing of *Foxc1*$^{h/h}$ mutant explants in media conditioned by WT meninges (right diagram).

(B–M) BrdU (red) and Ki-67 (green) double-immunolabeling of *Foxc1*$^{+/}$ and *Foxc1*$^{h/h}$ forebrain explants from the following treatment conditions: untreated Neurobasal media (NB) (B and C), meningeal transplantation (MT) (D and E), meningeal conditioned media (MCM) (F and G), atRA (H and I), MCM containing B27-VA supplement (J and K), and atRA-depleted MCM (L and M). Dotted line demarcates transition from proliferative and postmitotic zones in the cerebral wall. Unless noted otherwise, all media contained B27+VA supplement.

(N) Quantification of the percent BrdU^{+}/Ki-67^{-} in each explant treatment condition.

Scale bars = 50 μm. * indicates statistical significance from untreated *Foxc1*$^{+/}$ explants ($p < 0.05$). Error bars depict ± SEM.

(Zarbalis et al., 2007), did not colabel with Raldh2^{+} cells in the dorsal meninges (Figure 6E). In the ventral meninges, Foxc1 and Foxc2 both colocalized with meningeal Raldh2^{+} cells (Figures 6F and 6G).

Cortical Expansion Phenotype in *Rdh10* Hypomorph Mutants

To assess the requirement of atRA for corticogenesis, we used an *Rdh10* hypomorphic mutant that was recovered from the same ENU mutagenesis screen as the *Foxc1*$^{h/h}$ mice (Zarbalis et al., 2004) and that is viable to E16.5 (A.M.A. and A.P., unpublished data). These mice have eye, face, and limb defects that are very similar to a published *Rdh10* hypomorphic allele that is only viable until E13.5 (Sandell et al., 2007). Similar to the *Foxc1*$^{l/l}$ cortical phenotype (Figure 6J), the dorsal forebrain of the *Rdh10* mutant was much longer than that of its WT littermate at E13.5 (Figures 6H–6I), and the thickness of the postmitotic, Tuj1^{+} layer was reduced (Figures 6K–6M). Unlike the *Foxc1*$^{l/l}$, the Zic^{+} meninges appear intact in the *Rdh10* mutant (Figure S3). Analysis of Brn2 and Ctip2 at E16.5 revealed a thinned cortex

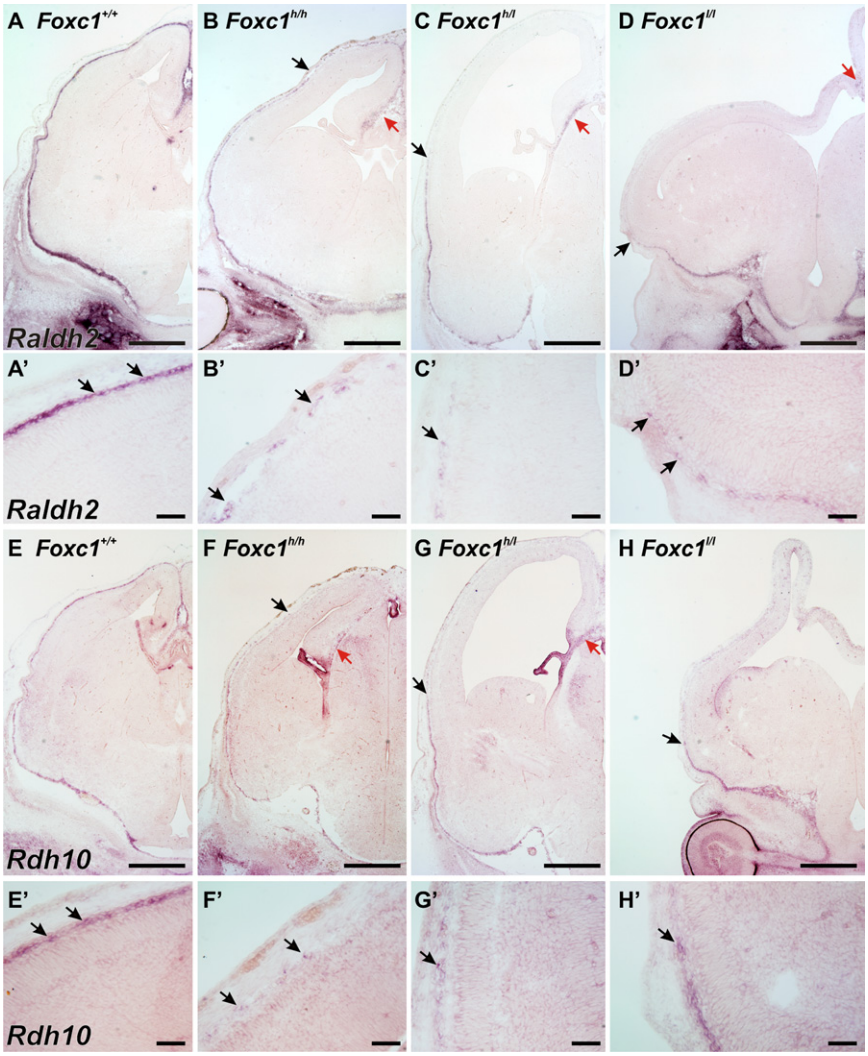

Figure 5. Expression of *Raldh2* and *Rdh10* in Wild-Type and *Foxc1* Mutant Meninges

Low-magnification (A–D) and high-magnification (A′–D′) images of in situ hybridization for *Raldh2* on E14.5 WT and *Foxc1* mutant heads. The endpoint of meningeal *Raldh2* signal is indicated by an arrow in (B)–(D). Red arrows in (B)–(D) indicate *Raldh2* signal in the midline correlating to residual meninges.

Low-magnification (E–H) and high-magnification (E′–H′) images of in situ hybridization for *Rdh10* on E14.5 WT and *Foxc1* mutant heads. The arrows in (F)–(H) indicate the end of *Rdh10* signal in the *Foxc1* mutants (magnified in F′–H′). Red arrows in (F) and (G) indicate *Rdh10* signal in the cortical hem and choroid plexus of $Foxc1^{h/h}$ and $Foxc1^{h/l}$ animals; it is not seen in the hem and choroid plexus of (H) as these structures are not present in the $Foxc1^{l/l}$ at this level.

Scale bars = 50 μm (A′–H′) and 500 μm (A–H). Arrows in (A′)–(H′) indicate cells with positive signal.

In Vivo Rescue of *Foxc1* Mutants by atRA Treatment

To examine in vivo rescue of the cortical phenotype, we injected 20 mg/kg atRA once daily into pregnant mice carrying $Foxc1^{h/h}$, $Foxc1^{h/l}$, or $Foxc1^{l/l}$ mutant embryos from E10.5 to E13.5 and collected them on E14.5. The atRA dosing regimen did not have any obvious effect on WT brains but led to a dramatic reduction in the dorsal forebrain length in the $Foxc1^{h/h}$ and $Foxc1^{h/l}$ mutants as compared to untreated mutants (Figures 7A–7F). Staining for Pax6 and Ctip2 untreated and atRA-treated brains highlights the decrease in the length of the neuroepithelium and increased thickness in the Ctip2$^+$, postmitotic population in the atRA-treated *Foxc1* mutants. Higher-magnification images of Ctip2 staining showed that atRA treatment did not affect generation of Ctip$^+$ neurons in WT cortices but increased the number of Ctip2$^+$ cells in the cerebral wall of $Foxc1^{h/h}$ and $Foxc1^{h/l}$ mutants as compared to untreated mutants (Figures 7I–7K). In the three litters analyzed, $Foxc1^{h/l}$ mutants showed a range of dorsal forebrain rescue (Figure S5A). Interestingly, the 20 mg/kg atRA dose did not rescue the cortical expansion phenotype in the $Foxc1^{l/l}$ mutant (data not shown). A higher dose of atRA (30mg/kg) reduced the length of the dorsal forebrain and increased the Ctip2$^+$ population as compared to the untreated $Foxc1^{l/l}$ mutant (Figures 7G, 7H, and 7L). Unfortunately, the higher dose of atRA also appeared to be toxic for the $Foxc1^{l/l}$ mutant embryos; in these brains, tissue integrity was compromised, the cells in the head and brain tissue appeared rounded, and there was activated caspase-3 in the head mesenchyme (Figure S5B). Zic immunolabeling in WT (Figures S4A and S4A′), $Foxc1^{h/l}$ (Figures S4B and S4B′), and $Foxc1^{l/l}$ (Figures S4C and S4C′) atRA exposed brains ruled out

in the *Rdh10* mutant with very few Ctip2 and Brn2$^+$ cells present (Figures 6N and 6O). The reduction in upper and lower cortical layer neurons was comparable to $Foxc1^{l/l}$ at E16.5 although the cortical layering was disorganized in the *Foxc1* mutant (Figure 6P).

To assess whether atRA is reduced in the $Foxc1^{l/l}$ mutant brains, total forebrain meninges or dorsal forebrain were collected separately from E14.5 $Foxc1^{l/l}$ brains and $Foxc1^{+/}$ littermates. Meningeal tissue collected from the $Foxc1^{l/l}$ brains contained significantly less atRA (~20%; $p < 0.05$) than littermate controls (Figure 6Q). The decline was likely not greater because it was difficult to only collect the tissue surrounding the cortex, thus Raldh2/Rdh10-expressing meninges from the midline and ventral forebrain $Foxc1^{l/l}$ meninges were included in the tissue dissected. An even greater decrease in atRA was observed in the $Foxc1^{l/l}$ cortices (~50%; $p < 0.05$). In addition, there was ~3-fold more atRA in the meninges than in the cortex (0.74 μmol/mg tissue versus 0.28 μmol/mg tissue in $Foxc1^{+/}$ samples).

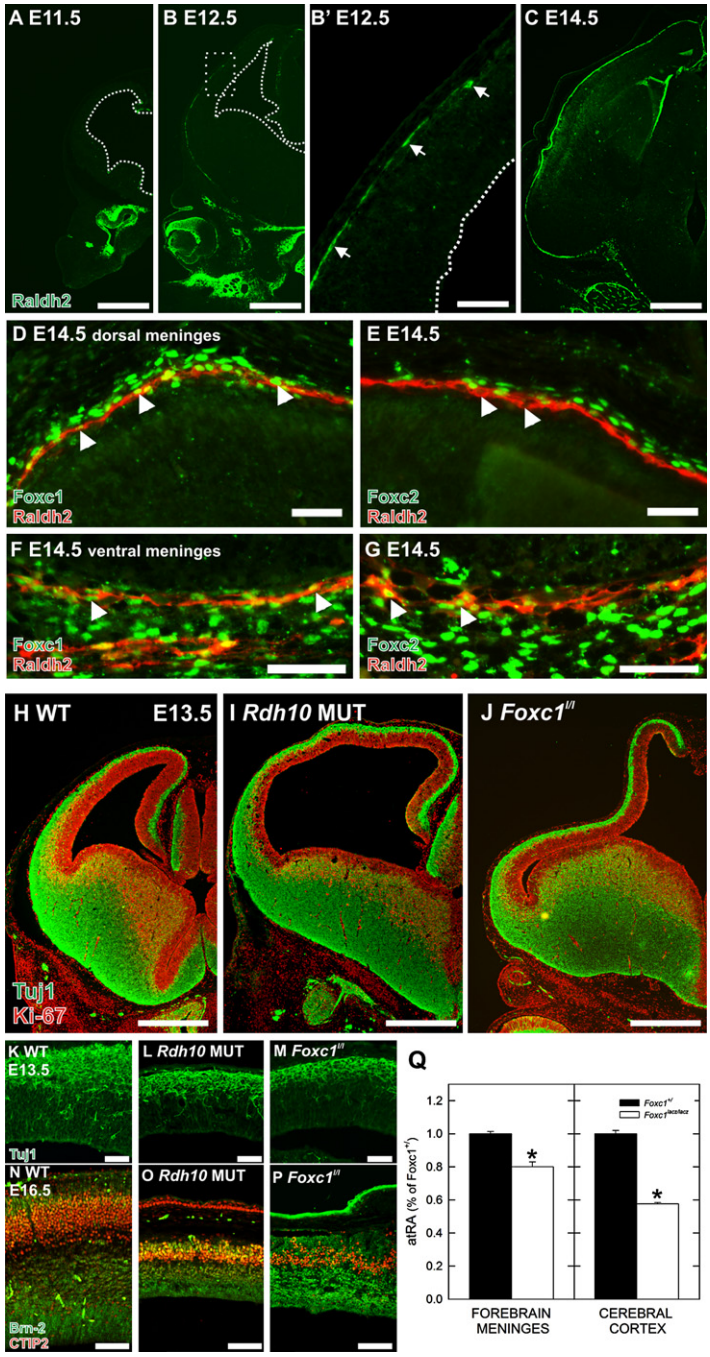

Figure 6. Raldh2 Expression in the Developing Meninges and Phenotype of *Rdh10* Mutant

(A–C) Raldh2 (green) expression at E11.5 (A), E12.5 (B), and (C) E14.5. Higher magnification of the box in (B) shows the leading edge of Raldh2 in the meninges (B′; arrows).

(D–G) High-magnification image of dorsal WT meninges at E14.5 showing expression of Foxc1 (green) in the nucleus of Raldh2 (red) expressing cells (D; arrows). Foxc2 is expressed in meningeal cells above the Raldh2 cell layer but Raldh2$^+$ cells in this area are not Foxc2$^+$ (E; arrows). In the ventral meninges, Raldh2$^+$ cells express both Foxc1 (F; arrows) and Foxc2 (G; arrows).

(H–J) Tuj1 (green) and Ki-67 (red) double-immunolabeling of E13.5 WT (H), *Rdh10* mutant (I), and *Foxc1*$^{l/l}$ (J) brains highlights the similarities in the dorsal forebrain phenotype in the two mutants.

(K–P) High-magnification images of Tuj1 (green; K–M) or dual Ctip2 (red) and Brn-2 (green; N–P) immunolabeling in E13.5 and E16.5 WT (K and N) *Rdh10* mutant (L and O) and *Foxc1*$^{l/l}$ mutant (M and P).

(Q) Graph depicting atRA levels in the total forebrain meninges and cortices of *Foxc1*$^{+/}$ and *Foxc1*$^{l/l}$ embryos at E14.5. Values are reported as percent of atRA in *Foxc1*$^{+/}$ tissue.

Scale bars = 50 μm (D, E, K, L, and M), 100 μm (N–P), 200 μm (F and G), and 500 μm (A–C, H–J). * indicates statistical significance from *Foxc1*$^{+/}$ ($p < 0.05$). Error bars depict ± SEM.

that the rescue of the *Foxc1* mutants was the result of an effect of atRA on the formation of the meninges.

To quantify the atRA rescue, the length of the dorsal forebrain and the number of Ctip$^+$ cells in a defined field were analyzed in atRA-treated WT and *Foxc1* mutant brains and compared to nontreated (NT) samples. atRA treatment significantly decreased ($p < 0.05$) the length of the dorsal forebrain (Figure 7M) and significantly increased ($p < 0.05$) the number of Ctip2$^+$ cells (Figure 7N) in all *Foxc1* mutants as compared to their NT counterparts. atRA-treated *Foxc1*$^{l/l}$ forebrains remained significantly longer ($p < 0.05$) (Figure 7M) and had significantly fewer ($p < 0.05$) Ctip2$^+$ cells than WT brains. In addition, atRA-treated *Foxc1*$^{h/h}$ and *Foxc1*$^{h/l}$ mutants showed significant improvement in neuron (Figures S5C and S5D) and IPC (Figures S5E and S5F) production as well as aPKCλ and Par3 expression (Figures S5G and S5H) compared to untreated mutants.

To test whether atRA supplementation also improves production of later generated neurons, we fed pregnant mice an atRA-enriched diet that allowed longer treatment times. The diet was less teratogenic than daily injections of atRA and the atRA-diet rescued *Foxc1*$^{h/h}$ and *Foxc1*$^{h/l}$ mutants at E14.5 to the same extent as the injections (data not shown). The *Foxc1*$^{h/l}$ mutant exposed to atRA from E10–E16.5 had a notable shorter, thicker cortex than the untreated mutant (Figure 7O). Analysis of Ctip2$^+$ and Brn2$^+$ in the neocortex confirmed a substantial increase in both early and late-generated neurons in the atRA-exposed *Foxc1*$^{h/l}$ mutant (Figure 7P). The lengthening of the neocortex was also improved in the atRA exposed (E10–E18.5) *Foxc1*$^{h/h}$ brain (Figure 7Q) as was generation of both Brn2$^+$ and Ctip2$^+$ neurons (Figure 7R); however there was still evidence of laminar disorganization in the atRA-exposed *Foxc1*$^{h/h}$ cortex. This is consistent with the cortical dysplasia observed in E18.5 *Foxc1*$^{h/h}$ mutants caused by meningeal/basement membrane defects that are likely present in the atRA-treated mutants.

DISCUSSION

Controlling the Timing and Progression of Neocortical Neurogenesis

The development of the mammalian neocortex is remarkable in that a cohort of progenitors undergoes multiple rounds of

division to produce a precisely defined set of distinct neuronal subtypes that occupy disparate cellular layers. The overall size of the cerebral cortex is controlled by the number of neuroepithelial progenitors generated via symmetric divisions and by the number of neurons that are generated from each progenitor via asymmetric divisions during the period of embryonic neuronogenesis (Caviness et al., 1995).

Though several proteins have been identified as central in the mechanics of the switch from symmetric to asymmetric divisions, few candidates have been identified that fit the criteria of a trigger event that signals to the VZ progenitors to begin undergoing neuronogenic divisions. The meninges are an ideal source of this signal, in part because their close proximity to the radial glial endfeet allows for a potent, short-range signal that need not influence IPC proliferation events (IPCs do not make contact with the glial limitans) or maturation of projection neurons in the cortical plate. Further, we have shown that the maturation of the meninges is such that the cells that make meningeal-derived atRA appear in a lateral-to-medial gradient as predicted for a signal responsible for the neurogenic gradient. From an evolutionary perspective, it is possible that the expansion of the neuroepithelium that is required to make a larger neocortex relies not only on events intrinsic to the neocortical neuroepithelium but also upon the timing of meningeal development, specifically the arrival of atRA-producing cells.

From our work and the work of others, a model of atRA in forebrain development emerges. During forebrain patterning and the earliest stages of cortical development prior to the arrival of Raldh2/Rdh10 cells in the meninges, atRA diffuses from the Raldh2, 3 enriched facial mesenchyme. Once corticogenesis proceeds in earnest, a more local source of atRA in the form of Raldh2/Rdh10 meningeal cells is required for neurogenic stimulation as the developing cortex is now spatially separated from atRA sources in the face (Figure 7S).

The Meninges Is a Signaling Center Regulating Brain Development

The idea of the meninges as a source of developmental cues is not a new concept. Previous studies showed that Cxcl12, a chemokine ligand, produced by the innermost layer of the meninges regulates the positioning of cortical interneurons and Cajal-Retzius cells by acting as a chemoattractant during corticogenesis (Borrell and Marin, 2006; Li et al., 2008; Lopez-Bendito et al., 2008; Paredes et al., 2006). The outermost layer of the meninges, the dura, is involved in the formation of the skull by releasing TGF-β family members and FGF-2 to induce bone formation (Ito et al., 2003; Mehrara et al., 1999). That we have identified atRA as a key component of the neurogenic signal produced by the middle meningeal layer now implicates all layers of the embryonic meninges as sources of cues that regulate the development of surrounding tissues. Further, the cranial neural crest origin of the meninges, a key source of the tremendous diversity of head structures seen in vertebrates (Le Douarin et al., 2007; Santagati and Rijli, 2003), suggests that the meninges may be an additional component of this evolutionary paradigm.

There is a possibility that the phenotype of the *Foxc1* mutants may be related to the vascular phenotype that is seen in these mice. For example, endothelial cells secrete factors like FGF that stimulate embryonic neural stem cells to undergo symmetric, self-renewing divisions (Shen et al., 2004). Foxc1, however, is expressed in pericytes and smooth muscle cells in the meninges and cortical vasculature but not by endothelial cells (J.A.S. and S.J.P., unpublished data). Also, the vascular defects do not appear until after the cortical phenotype is apparent in the *Foxc1* mutants. There may be a pericyte-derived factor that influences neurogenesis that is not produced in the absence of Foxc1. This is unlikely given that mouse mutants that have severely reduced pericyte numbers in the developing cortex do not have a cortical phenotype (Hellstrom et al., 2001).

atRA as a Sequential Inducer of Forebrain Development

atRA is an ideal molecule to induce neuronogenic divisions because it is a potent neural differentiation signal. Treatment of embryonic stem cells with atRA triggers upregulation of a series of neural-specific genes that ultimately results in the production of both neurons and glia (Maden, 2001). Because it is such a strong neuronal induction cue, restricting atRA production to the meninges may prevent inappropriate atRA signaling. In support of this, CRABP I, II and CRBP1, proteins that bind and chaperone atRA and retinol, respectively (Napoli, 1999), are expressed by the meninges during development, when they may further titrate atRA exposure of the radial glial endfeet (Ruberte et al., 1993). In addition, CRABP II is expressed in the VZ of the developing cortex (Ruberte et al., 1993), where it likely aids in the intracellular transport of atRA to the nucleus through the cytoplasm of the radial glial fiber. This model of restricted atRA exposure has already been established in the hindbrain. atRA signaling in hindbrain is limited to migrating cells and fixed structures adjacent to the regions of Raldh2-enriched meninges (Zhang et al., 2003).

Despite the fact that atRA is a well-recognized cue for neuronal differentiation, a function for this molecule in neocortical development has been difficult to establish because the key mutants in the signaling pathways exhibit phenotypes at earlier stages of forebrain development and die before corticogenesis begins (Ribes et al., 2006). However, although not noted in the original publication, in RARα/γ double-knockout the dorsal forebrain is elongated in a manner similar to the *Rdh10* and *Foxc1*$^{-/-}$ mutants (Figure 2h in Lohnes et al., 1994). Also, vitamin A deprivation from E11 to E13 results in a reduction in postmitotic neurons in the telencephalon (Dickman et al., 1997). These data are consistent with our analysis of the cortical phenotype in the *Rdh10* mutants. The *Rdh10* mutants appear to have meninges covering the cortex that presumably produce and secrete other meningeal-derived cues like CXCL12 but are not capable of producing normal levels of atRA. This provides further evidence that atRA is the primary signal from the meninges regulating corticogenesis.

Transgenic retinoic acid response element-*lacZ* reporter mice (*RARE-lacZ*) are frequently used to assess retinoid signaling in the developing embryo and have a strong β-gal signal in radial glial cells in the forebrain (Haskell and LaMantia, 2005; Luo et al., 2004). Our analysis of the *RARE-hsp68lacZ* transgene (Rossant et al., 1991) in *Foxc1*$^{+/-}$ and *Foxc1*$^{-/-}$ brains revealed that most of the β-gal observed in the dorsal forebrain persists from transgene activation from an earlier developmental stage

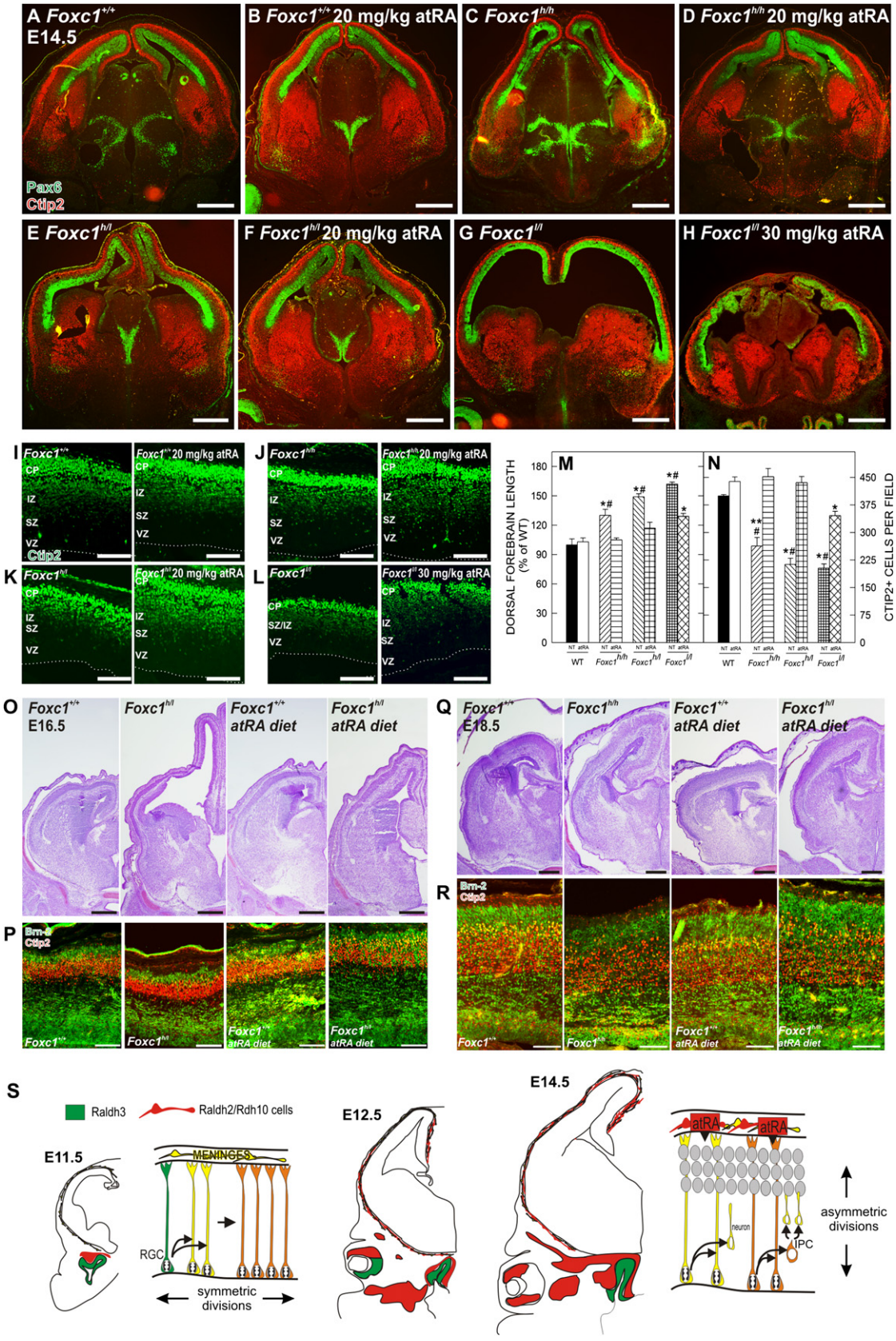
A Foxc1+/+ E14.5
B Foxc1+/+ 20 mg/kg atRA
C Foxc1h/h
D Foxc1h/h 20 mg/kg atRA
Pax6
Ctip2
E Foxc1h/l
F Foxc1h/l 20 mg/kg atRA
G Foxc1l/l
H Foxc1l/l 30 mg/kg atRA
I
J
K
L
CP
IZ
SZ
VZ
SZ/IZ
M
N
DORSAL FOREBRAIN LENGTH (% of WT)
CTIP2+ CELLS PER FIELD
NT
atRA
WT
O
E16.5
atRA diet
P
Brn-2
Ctip2
Q
E18.5
R
S
Raldh3
Raldh2/Rdh10 cells
E11.5
MENINGES
RGC
symmetric divisions
E12.5
E14.5
atRA
neuron
IPC
asymmetric divisions

(data not shown). Indeed, *Raldh2*$^{-/-}$;*RARE-lacZ* embryos, when given atRA to avoid early lethality, show persistent β-gal activity in the dorsal forebrain potentially resulting from early exposure to atRA produced from Raldh3-expressing olfactory placodes (Niederreither et al., 2002). In light of all the evidence implicating atRA in cortical development, our observation of low *RARE-lacZ* activation (as assayed by *lacZ* in situ probe) in the *Foxc1*$^{+/l}$ cortices is not an accurate picture of the role of atRA signaling during corticogenesis and thus is not useful in assessing whether atRA signaling is altered in the *Foxc1*$^{l/l}$ mutants. The low *RARE-lacZ* activation, despite the presence of atRA in the cortex, may be a result of the high levels of RARE repressive activity in the developing cortex, even in the presence of atRA which normally relieves transcriptional repression of RAREs by RAR/RXR heterodimers (Liao et al., 2005). Also, the two *RARE-lacZ* transgenes (*RARE-hsp68lacZ* [Rossant et al., 1991] and RARE/tk/β-gal [Balkan et al., 1992]) both employ the RARE of the RARβ2 gene promoter. Previous studies showed that specific RAR/RXR cofactors are intimately involved in both the activation and repression of the RARE specific to the RARβ2 promotor (Folkers et al., 1998). Thus the absence or overabundance of these cofactors in the forebrain likely influence the *RARE-lacZ* transgene activation and could lead to false positives and negatives with regard to retinoid signaling.

Summary

The *Foxc1* mutants provide a unique opportunity to assess forebrain development in which a very discrete head structure, the forebrain meninges, is reduced or completely absent. As a result, we were able to identify a previously unknown role for the meninges: promotion of cortical neuron generation through release of a bioactive molecule. The identification of atRA as the bioactive signal from the meninges is compelling, providing impetus to pursue the details of atRA signaling in the VZ and to determine the mechanism of control of the neuronogenic decision by atRA at this time.

EXPERIMENTAL PROCEDURES

Animals

Details of animal breeding, atRA treatment, and genotyping are found in the Supplemental Data.

Cell-Cycle Exit, Tbr2, Ctip2, and Cerebral Length Analysis

For cell-cycle exit analysis, the pregnant dam was injected with BrdU (50 mg/kg b.w.) on E13. Fetuses were harvested 18 hr following the injection and the heads were processed for BrdU/Ki-67 double immunolabeling. The fraction of cells that had exited the cell cycle was estimated by counting the number of BrdU$^+$ cells in a 200 μm portion of the dorsal forebrain and the number of BrdU$^+$/Ki-67$^-$ cells in the same area. The cell-cycle exit fraction reported is the number of BrdU$^+$/Ki-67$^-$ cells divided by the total number of BrdU$^+$ cells. For analysis of the Tbr2 and Ctip2 population, the total number of Tbr2$^+$ or Ctip2$^+$ cells in a 200 μm portion of the dorsal forebrain was counted. Care was taken to ensure that the population analyzed was at a comparable rostral/caudal and lateral/medial position in each of the samples. Analysis of dorsal forebrain length consisted of measuring the length of the ventricular surface from the pallial-subpallial border to the tip of cortical hem in sections from a similar rostral/caudal position. For each untreated and atRA-treated genotype, cell-cycle exit, Tbr2, Ctip2, and cerebral length analysis was performed on sections from a minimum of three WT brains and three brains from each mutant line from a minimum of two separate litters ($n \geq 2$).

Forebrain Explants and Meningeal Cultures

Detailed methods of explant methods and meningeal cultures are in the Supplemental Data.

In Situ Hybridization

Raldh2 and *Rdh10* in situ hybridization was performed as previously described (Zarbalis and Wurst, 2000). ISH with *Rdh10* was performed using a 900 bases long DIG-labeled riboprobe comprising coding sequences and 3′UTR. DIG-labeled riboprobe for *Raldh2* was transcribed from a plasmid containing 937 bp of coding sequence and 3′UTR kindly provided by Dr. John L.R. Rubenstein.

Immunohistochemistry and X-Gal Staining

Whole embryo or whole head from E10.5–E16.5 were collected and fixed overnight at 4°C in 4% paraformaldehyde, cryoprotected, and frozen in OCT. E18.5 heads were either fresh frozen in OCT or fixed as described above. Tissue was cryosectioned in 12 μm increments. Immunostaining was performed as described previously (Zarbalis et al., 2007) using the following antibodies and concentrations: mouse anti-BrdU 1:50, BD Bioscience; rat anti-BrdU 1:300, Novus; mouse anti-Tuj1 1:1000, Covance; rabbit anti-Zic 1:1500, gift from J. Aruga RIKEN Institute; rabbit anti-Raldh2 1:1000, gift from P. McCaffery, University of Aberdeen; rabbit anti-Ki-67 1:300, LabVision; rabbit anti-Tbr2 1:300, Chemicon; rat anti-Ctip2 1:800, Abcam; rabbit anti-Brn2 1:200, Santa Cruz Biotechnologies; goat anti-Foxc1 1:300, Novus Biologicals; goat anti-Foxc2 1:300, Novus Biologicals. For x-gal staining, heads were fixed for 1 hr in 4% paraformaldehyde, cryoprotected, and cut in 25 μm increments. Sections were stained overnight with 1 mg/ml x-gal solution (Sigma). All immunofluorescent and brightfield images were captured using a Retiga CCD-cooled camera and associated QCapture Pro software (QImaging Surrey). For quantification of the Par3 and aPKCλ immunofluorescence, the mean gray value was calculated using ImageJ software (NIH) and the values were reported in the graphs as arbitrary units (a.u.). Analyzed images were from three brains from at least two litters for each genotype/treatment condition ($n \geq 2$).

Statistics

For pairwise analysis of treatment conditions and/or genotypes, Student's t tests were used. The standard errors of the mean (SEM) (±) are reported on all graphs.

Figure 7. In Vivo Rescue of *Foxc1* Forebrain Phenotype by atRA

(A–H) Ctip2 (green) and Pax6 (red) immunostaining on E14.5 untreated (A, C, E, and G) and atRA-treated (B, D, F, and H) WT and *Foxc1* mutants.

(I–L) Ctip2 immunostaining in untreated and atRA-treated WT (I), *Foxc1*$^{h/h}$ (J), *Foxc1*$^{h/l}$ (K), and *Foxc1*$^{l/l}$ (L) at E14.5. Dotted line indicates ventricular surface.

(M) Quantification of the dorsal forebrain length; values are a percentage of the mean length of untreated WT.

(N) Quantification of Ctip2$^+$ cells in untreated and atRA-treated WT and *Foxc1* mutant cortices.

(O–P) Nissl-stained E16.5 brains from untreated WT and *Foxc1*$^{h/l}$ and embryos exposed to an atRA diet (O). Adjacent sections immunolabeled for Ctip2 (red) and Brn-2 (green) (P).

(Q–R) Nissl staining (Q) and Ctip2 (red) and Brn-2 (green) immunolabeling (R) from untreated and atRA diet E18.5 WT and *Foxc1*$^{h/h}$ brains.

(S) Schematic of cortical neuroepithelial divisions prior to (E11.5) and after (E14.5) the arrival of Raldh2/Rdh10-expressing cells (red cells) in the meninges.

Scale bars = 500 μm (A–H, O, and Q) and 100 μm (I–L, P, and R). *#, *, and **# indicate statistical significance ($p < 0.05$) from both untreated/atRA-treated WT and atRA-treated *Foxc1* mutants, untreated/atRA-treated WT, and untreated *Foxc1*$^{h/l}$ and *Foxc1*$^{l/l}$, respectively. Error bars depict ± SEM.

SUPPLEMENTAL DATA

Supplemental Data include Supplemental Experimental Procedures and five figures and can be found with this article online at http://www.cell.com/supplemental/S0092-8674(09)01252-5.

ACKNOWLEDGMENTS

We thank Dr. Grant Li for technical assistance and helpful discussions, Dr. Brad Pawlikowski for critical review of the manuscript, and Drs. John Rubenstein and Arturo Alvarez-Buylla for helpful discussion. This work was supported by grants from the NIH (R01DA017627), Autism Speaks, and the AHA/AAN.

Received: September 7, 2008
Revised: July 10, 2009
Accepted: September 1, 2009
Published: October 29, 2009

REFERENCES

Anchan, R.M., Drake, D.P., Haines, C.F., Gerwe, E.A., and LaMantia, A.S. (1997). Disruption of local retinoid-mediated gene expression accompanies abnormal development in the mammalian olfactory pathway. J. Comp. Neurol. *379*, 171–184.

Balkan, W., Colbert, M., Bock, C., and Linney, E. (1992). Transgenic indicator mice for studying activated retinoic acid receptors during development. Proc. Natl. Acad. Sci. USA *89*, 3347–3351.

Borrell, V., and Marin, O. (2006). Meninges control tangential migration of hem-derived Cajal-Retzius cells via CXCL12/CXCR4 signaling. Nat. Neurosci. *9*, 1284–1293.

Caviness, V.S., Jr., Takahashi, T., and Nowakowski, R.S. (1995). Numbers, time and neocortical neuronogenesis: a general developmental and evolutionary model. Trends Neurosci. *18*, 379–383.

Chambon, P. (1996). A decade of molecular biology of retinoic acid receptors. FASEB J. *10*, 940–954.

Chenn, A., and McConnell, S.K. (1995). Cleavage orientation and the asymmetric inheritance of Notch1 immunoreactivity in mammalian neurogenesis. Cell *82*, 631–641.

Chenn, A., and Walsh, C.A. (2002). Regulation of cerebral cortical size by control of cell cycle exit in neural precursors. Science *297*, 365–369.

Costa, M.R., Wen, G., Lepier, A., Schroeder, T., and Gotz, M. (2008). Par-complex proteins promote proliferative progenitor divisions in the developing mouse cerebral cortex. Development *135*, 11–22.

Dickman, E.D., Thaller, C., and Smith, S.M. (1997). Temporally-regulated retinoic acid depletion produces specific neural crest, ocular and nervous system defects. Development *124*, 3111–3121.

Dolle, P., Fraulob, V., Kastner, P., and Chambon, P. (1994). Developmental expression of murine retinoid X receptor (RXR) genes. Mech. Dev. *45*, 91–104.

Folkers, G.E., van der Burg, B., and van der Saag, P.T. (1998). Promoter architecture, cofactors, and orphan receptors contribute to cell-specific activation of the retinoic acid receptor β2 promoter. J. Biol. Chem. *273*, 32200–32212.

Haskell, G.T., and LaMantia, A.S. (2005). Retinoic acid signaling identifies a distinct precursor population in the developing and adult forebrain. J. Neurosci. *25*, 7636–7647.

Hellstrom, M., Gerhardt, H., Kalen, M., Li, X., Eriksson, U., Wolburg, H., and Betsholtz, C. (2001). Lack of pericytes leads to endothelial hyperplasia and abnormal vascular morphogenesis. J. Cell Biol. *153*, 543–553.

Inoue, T., Ogawa, M., Mikoshiba, K., and Aruga, J. (2008). Zic deficiency in the cortical marginal zone and meninges results in cortical lamination defects resembling those in type II lissencephaly. J. Neurosci. *28*, 4712–4725.

Ito, Y., Yeo, J.Y., Chytil, A., Han, J., Bringas, P., Jr., Nakajima, A., Shuler, C.F., Moses, H.L., and Chai, Y. (2003). Conditional inactivation of Tgfßr2 in cranial neural crest causes cleft palate and calvaria defects. Development *130*, 5269–5280.

Kane, M.A., Chen, N., Sparks, S., and Napoli, J.L. (2005). Quantification of endogenous retinoic acid in limited biological samples by LC/MS/MS. Biochem. J. *388*, 363–369.

Kane, M.A., Folias, A.E., Wang, C., and Napoli, J.L. (2008). Quantitative profiling of endogenous retinoic acid in vivo and in vitro by tandem mass spectrometry. Anal. Chem. *80*, 1702–1708.

Kawaguchi, A., Ogawa, M., Saito, K., Matsuzaki, F., Okano, H., and Miyata, T. (2004). Differential expression of Pax6 and Ngn2 between pair-generated cortical neurons. J. Neurosci. Res. *78*, 784–795.

Kume, T., Deng, K.Y., Winfrey, V., Gould, D.B., Walter, M.A., and Hogan, B.L. (1998). The forkhead/winged helix gene Mf1 is disrupted in the pleiotropic mouse mutation congenital hydrocephalus. Cell *93*, 985–996.

Le Douarin, N.M., Brito, J.M., and Creuzet, S. (2007). Role of the neural crest in face and brain development. Brain Res. Brain Res. Rev. *55*, 237–247.

Li, G., Adesnik, H., Li, J., Long, J., Nicoll, R.A., Rubenstein, J.L., and Pleasure, S.J. (2008). Regional distribution of cortical interneurons and development of inhibitory tone are regulated by Cxcl12/Cxcr4 signaling. J. Neurosci. *28*, 1085–1098.

Li, W., Cogswell, C.A., and LoTurco, J.J. (1998). Neuronal differentiation of precursors in the neocortical ventricular zone is triggered by BMP. J. Neurosci. *18*, 8853–8862.

Liao, W.L., Wang, H.F., Tsai, H.C., Chambon, P., Wagner, M., Kakizuka, A., and Liu, F.C. (2005). Retinoid signaling competence and RARβ-mediated gene regulation in the developing mammalian telencephalon. Dev. Dyn. *232*, 887–900.

Lohnes, D., Mark, M., Mendelsohn, C., Dolle, P., Dierich, A., Gorry, P., Gansmuller, A., and Chambon, P. (1994). Function of the retinoic acid receptors (RARs) during development (I). Craniofacial and skeletal abnormalities in RAR double mutants. Development *120*, 2723–2748.

Lopez-Bendito, G., Sanchez-Alcaniz, J.A., Pla, R., Borrell, V., Pico, E., Valdeolmillos, M., and Marin, O. (2008). Chemokine signaling controls intracortical migration and final distribution of GABAergic interneurons. J. Neurosci. *28*, 1613–1624.

Luo, T., Wagner, E., Grun, F., and Drager, U.C. (2004). Retinoic acid signaling in the brain marks formation of optic projections, maturation of the dorsal telencephalon, and function of limbic sites. J. Comp. Neurol. *470*, 297–316.

Maden, M. (2001). Role and distribution of retinoic acid during CNS development. Int. Rev. Cytol. *209*, 1–77.

Mehrara, B.J., Most, D., Chang, J., Bresnick, S., Turk, A., Schendel, S.A., Gittes, G.K., and Longaker, M.T. (1999). Basic fibroblast growth factor and transforming growth factor β-1 expression in the developing dura mater correlates with calvarial bone formation. Plast. Reconstr. Surg. *104*, 435–444.

Miyata, T., Kawaguchi, A., Saito, K., Kawano, M., Muto, T., and Ogawa, M. (2004). Asymmetric production of surface-dividing and non-surface-dividing cortical progenitor cells. Development *131*, 3133–3145.

Molotkova, N., Molotkov, A., and Duester, G. (2007). Role of retinoic acid during forebrain development begins late when Raldh3 generates retinoic acid in the ventral subventricular zone. Dev. Biol. *303*, 601–610.

Napoli, J.L. (1999). Interactions of retinoid binding proteins and enzymes in retinoid metabolism. Biochim. Biophys. Acta *1440*, 139–162.

Napoli, J.L. (2004). Vitamin A (Retinoids), Volume 4 (New York: Elsiever Ltd.).

Niederreither, K., Subbarayan, V., Dolle, P., and Chambon, P. (1999). Embryonic retinoic acid synthesis is essential for early mouse post-implantation development. Nat. Genet. *21*, 444–448.

Niederreither, K., Vermot, J., Fraulob, V., Chambon, P., and Dolle, P. (2002). Retinaldehyde dehydrogenase 2 (RALDH2)-independent patterns of retinoic acid synthesis in the mouse embryo. Proc. Natl. Acad. Sci. USA *99*, 16111–16116.

Noctor, S.C., Martinez-Cerdeno, V., Ivic, L., and Kriegstein, A.R. (2004). Cortical neurons arise in symmetric and asymmetric division zones and migrate through specific phases. Nat. Neurosci. *7*, 136–144.

Noctor, S.C., Martinez-Cerdeno, V., and Kriegstein, A.R. (2008). Distinct behaviors of neural stem and progenitor cells underlie cortical neurogenesis. J. Comp. Neurol. *508*, 28–44.

Paredes, M.F., Li, G., Berger, O., Baraban, S.C., and Pleasure, S.J. (2006). Stromal-derived factor-1 (CXCL12) regulates laminar position of Cajal-Retzius cells in normal and dysplastic brains. J. Neurosci. *26*, 9404–9412.

Qian, X., Davis, A.A., Goderie, S.K., and Temple, S. (1997). FGF2 concentration regulates the generation of neurons and glia from multipotent cortical stem cells. Neuron *18*, 81–93.

Ribes, V., Wang, Z., Dolle, P., and Niederreither, K. (2006). Retinaldehyde dehydrogenase 2 (RALDH2)-mediated retinoic acid synthesis regulates early mouse embryonic forebrain development by controlling FGF and sonic hedgehog signaling. Development *133*, 351–361.

Romand, R., Kondo, T., Cammas, L., Hashino, E., and Dolle, P. (2008). Dynamic expression of the retinoic acid-synthesizing enzyme retinol dehydrogenase 10 (Rdh10) in the developing mouse brain and sensory organs. J. Comp. Neurol. *508*, 879–892.

Ross, S.A., McCaffery, P.J., Drager, U.C., and De Luca, L.M. (2000). Retinoids in embryonal development. Physiol. Rev. *80*, 1021–1054.

Rossant, J., Zirngibl, R., Cado, D., Shago, M., and Giguere, V. (1991). Expression of a retinoic acid response element-hsplacZ transgene defines specific domains of transcriptional activity during mouse embryogenesis. Genes Dev. *5*, 1333–1344.

Ruberte, E., Friederich, V., Chambon, P., and Morriss-Kay, G. (1993). Retinoic acid receptors and cellular retinoid binding proteins. III. Their differential transcript distribution during mouse nervous system development. Development *118*, 267–282.

Sandell, L.L., Sanderson, B.W., Moiseyev, G., Johnson, T., Mushegian, A., Young, K., Rey, J.P., Ma, J.X., Staehling-Hampton, K., and Trainor, P.A. (2007). RDH10 is essential for synthesis of embryonic retinoic acid and is required for limb, craniofacial, and organ development. Genes Dev. *21*, 1113–1124.

Santagati, F., and Rijli, F.M. (2003). Cranial neural crest and the building of the vertebrate head. Nat. Rev. Neurosci. *4*, 806–818.

Shen, Q., Goderie, S.K., Jin, L., Karanth, N., Sun, Y., Abramova, N., Vincent, P., Pumiglia, K., and Temple, S. (2004). Endothelial cells stimulate self-renewal and expand neurogenesis of neural stem cells. Science *304*, 1338–1340.

Vivatbutsiri, P., Ichinose, S., Hytonen, M., Sainio, K., Eto, K., and Iseki, S. (2008). Impaired meningeal development in association with apical expansion of calvarial bone osteogenesis in the *Foxc1* mutant. J. Anat. *212*, 603–611.

Zarbalis, K., and Wurst, W. (2000). Expression domains of murine ephrin-A5 in the pituitary and hypothalamus. Mech. Dev. *93*, 165–168.

Zarbalis, K., May, S.R., Shen, Y., Ekker, M., Rubenstein, J.L., and Peterson, A.S. (2004). A focused and efficient genetic screening strategy in the mouse: identification of mutations that disrupt cortical development. PLoS Biol. *2*, E219. 10.1371/journal.pbio.0020219.

Zarbalis, K., Siegenthaler, J.A., Choe, Y., May, S.R., Peterson, A.S., and Pleasure, S.J. (2007). Cortical dysplasia and skull defects in mice with a *Foxc1* allele reveal the role of meningeal differentiation in regulating cortical development. Proc. Natl. Acad. Sci. USA *104*, 14002–14007.

Zhang, J., Smith, D., Yamamoto, M., Ma, L., and McCaffery, P. (2003). The meninges is a source of retinoic acid for the late-developing hindbrain. J. Neurosci. *23*, 7610–7620.